THE JOURNAL OF PHYSICAL CHEMISTRY Letters

PERSPECTIVE

pubs.acs.org/JPCL

Elucidating Peptide and Protein Structure and Dynamics: UV Resonance Raman Spectroscopy

Sulayman A. Oladepo, Kan Xiong, Zhenmin Hong, and Sanford A. Asher*

Department of Chemistry, University of Pittsburgh, Pittsburgh, Pennsylvania 15260, United States

ABSTRACT UV resonance Raman spectroscopy (UVRR) is a powerful method that has the requisite selectivity and sensitivity to incisively monitor biomolecular structure and dynamics in solution. In this Perspective, we highlight applications of UVRR for studying peptide and protein structure and the dynamics of protein and peptide folding. UVRR spectral monitors of protein secondary structure, such as the amide III_3 band and the C_α—H band frequencies and intensities, can be used to determine Ramachandran Ψ angle distributions for peptide bonds. These incisive, quantitative glimpses into conformation can be combined with kinetic *T*-jump methodologies to monitor the dynamics of biomolecular conformational transitions. The resulting UVRR structural insight is impressive in that it allows differentiation of, for example, different α-helix-like states that enable differentiating π and 3_{10} states from pure α-helices. These approaches can be used to determine the Gibbs free-energy landscape of individual peptide bonds along the most important protein (un)folding coordinate. Future work will find spectral monitors that probe peptide bond activation barriers that control protein (un)folding mechanisms. In addition, UVRR studies of side chain vibrations will probe the role of side chains in determining protein secondary, tertiary, and quaternary structures.

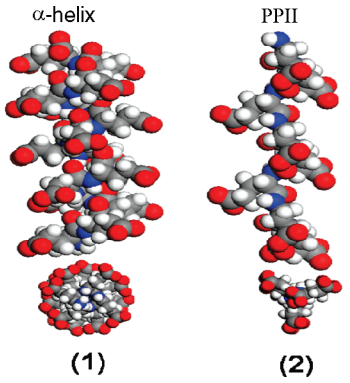

Protein Folding Problem. An understanding of the mechanism(s) of protein folding, whereby the ribosome-synthesized biopolymer folds into its native protein, is arguably one of the most important unsolved problems in biology.[1−7] The primary sequence of many or most proteins encodes both the native structure as well as the folding mechanism pathway to the native structure.[8−10] An understanding of the encoded protein folding "rules" would dramatically speed insight into protein structure and function.

An understanding of the encoded protein folding "rules" would dramatically speed insight into protein structure and function.

A number of mechanisms have been proposed that differ in the order of folding events. The framework model[11] and the diffusion−collision model[12] propose that the initial step in folding involves formation of native-like secondary structural units, while the hydrophobic collapse model and the nucleation−condensation model[13] suggest that hydrophobic or nucleating domains fold first and that these structures drive the subsequent formation of secondary structure. Recent energy landscape models[14] propose the occurrence of funnel-shaped folding energy landscapes, where the native state is accessed via a strategically sloped energy landscape that funnels myriads of partially folded conformations toward the native folded state.[15]

Techniques for Studying Protein Folding. Numerous experimental techniques are being applied to study protein folding. In addition, various theoretical approaches are also being utilized with empirically developed parameters to try to get insight into the folding mechanisms.[16] UV−visible absorption spectroscopy was the first technique used to monitor the UV absorption of the peptide backbone. This method was able to detect protein backbone conformational changes because of the hypo- and hyperchromic interactions that, for example, result from peptide bond excitonic interactions in the α-helix conformation.[17,18] The development of circular dichroism spectroscopy enabled more direct monitoring of protein secondary structural content, especially the occurrence of α-helical conformations.[19]

X-ray Crystallography is the gold standard technique for determining static protein structures (from protein crystals), and much of the insight into protein science has resulted from the many incisive stationary X-ray structures. However, these static X-ray structures do not give the dynamic structural information essential to determine enzymatic mechanisms, for example.

Nuclear magnetic resonance spectroscopy (NMR) is an extraordinarily powerful tool for studying protein folding.[20]

Received Date: December 1, 2010
Accepted Date: January 20, 2011
Published on Web Date: February 17, 2011

DOI: 10.1021/jz101619f | *J. Phys. Chem. Lett.* 2011, *2*, 334–344

The technique is also capable of elucidating detailed aspects of the structure and dynamics of large proteins. However, the atomic distances and dihedral angles measured by this technique are generally time averages.[21]

Laser spectroscopy techniques enable highly incisive structural investigations that can be utilized to study dynamics in the femtosecond to static time scales. IR and Raman vibrational spectroscopies can monitor small changes in protein structure resulting from tiny ~0.001 nm bond length changes. Unfortunately, the use of IR absorption spectroscopy is challenging for biological samples because it is generally limited to D_2O solution samples due to the overwhelming IR absorption of H_2O.[22]

Raman spectroscopy monitors the vibrations of gas, liquid, and solid samples.[23−25] H_2O is a relatively weak Raman scatterer. This enables Raman studies of biological molecules in H_2O. Raman spectroscopy is an inelastic light-scattering phenomenon where the incident electromagnetic field interacts with a molecule such that there is an exchange of a quantum of vibrational energy between the two, resulting in a vibrational frequency difference between the incident and scattered light.[26−35] In normal or off-resonance Raman scattering, the incident photon at a frequency outside of any electronic absorption band is inelastically scattered, leaving the molecule in an excited vibrational level of the electronic ground state (for Stokes scattering). A similar vibrational transition occurs for resonance Raman scattering, where excitation occurs at a frequency within an electronic absorption band. In this case, the vibrational modes observed are particular vibrations whose motions couple to the driven electronic motion occurring in the electronic transition. The vibrational modes enhanced are those localized in the chromophoric segments.

The additional *resonance* Raman enhancement can be an additional 10^6-10^8-fold. This results in a crucial ultrahigh resonance Raman selectivity and sensitivity that makes it a very powerful technique for studying macromolecules; instead of all of the sample vibrations contributing with comparable intensities, only a small subset of resonance Raman-enhanced vibrations localized around the chromophoric group dominate the spectra. By judiciously tuning the excitation wavelength, we can selectively enhance particular vibrations in particular regions of the macromolecule.[36,37] Figure 1 demonstrates the UVRR selectivity available, for example, for studying the protein myoglobin (Mb).[38,39] The visible wavelength absorption bands of Mb result from the in-plane $\pi \rightarrow \pi^*$ electronic transitions of its heme group. Resonance Raman (RR) excitation of Mb at 415 nm in the strong heme Soret absorption band results in an intense RR spectra which contains only the in-plane heme ring vibrations.[40] In contrast, excitation at 229 nm within the absorption bands of the Tyr and Trp aromatic side chains shows RR spectra completely dominated by Tyr and Trp aromatic ring side chain vibrations.[39,41] Deeper UV excitation at 206.5 nm, within the $\pi \rightarrow \pi^*$ transitions of the amide peptide bonds, shows UVRR spectra dominated by the peptide bond amide vibrations.[39]

Thus, tuning the UVRR excitation wavelengths allows the probing of different chromophoric segments of a macromolecule. Another advantage of deep UV Raman measurements

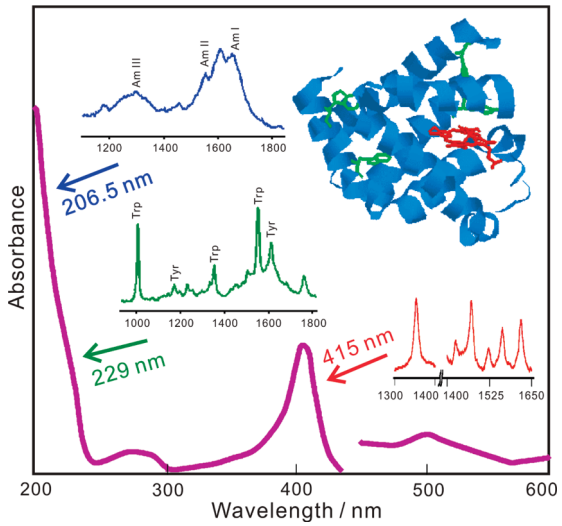

Figure 1. Selectivity of resonance Raman spectral measurements of myoglobin showing the protein absorption spectrum and the different resonance Raman spectra obtained with different excitation wavelengths.

is that there is no interference from molecular relaxed fluorescence.[42] In addition, UVRR can also be used in pump−probe measurements to give kinetic information on fast biological processes.[43]

UVRR Instrumentation. The rapid development of UVRR has been aided by recent advances in lasers, optics, and detectors. For temperature-jump (*T*-jump) measurements, an IR pump pulse at 1.9 μm excites the overtone absorption band of water and heats a small sample volume. A time-delayed UV probe pulse excites the UVRR of the IR-pulse-heated volume. The UVRR light is collected and dispersed by a spectrograph, and the spectrum is detected by a CCD detector. Non-kinetic Raman measurements of static structure are best measured by using CW lasers that avoid nonlinear optical and thermal processes that can induce sample degradation.[44]

However, high repetition rate (1−5 kHz) pulsed (10−50 ns) Nd:YLF pumped Ti:Sapphire lasers[43,45] are very convenient UVRR laser sources because their output can be easily and continuously tuned between 193 and 240 nm. These deep-UV excitation beams are generated by frequency quadrupling or tripling and mixing the Ti:Sapphire laser fundamentals. Liquid-nitrogen-cooled CCD cameras are the optimum UVRR detector because of their low noise.

Protein and Peptide Bond Studies. UV excitation involves the HOMO and LUMO molecular orbitals of the peptide bond (secondary amides, except for proline). The lowest-energy $n \rightarrow \pi^*$ transition at ~220 nm is electronically forbidden and weak. It gives rise to the strong CD signature of the α-helix conformation but gives rise to negligible resonance Raman enhancement.[19,46] The ~190 nm $\pi \rightarrow \pi^*$ transition is strongly allowed, with a strong absorption band that gives rise to strong UVRR intensities.[47] Excitation within this absorption band gives rise to the strong UVRR enhancement of vibrations that have large components of C—N stretching. A somewhat smaller enhancement occurs for vibrations with strong C═O stretching.[48]

DOI: 10.1021/jz101619f | *J. Phys. Chem. Lett.* 2011, *2*, 334–344

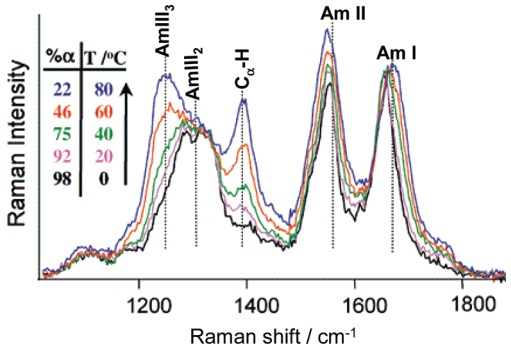

Figure 2. The temperature dependence of the UVRR spectra and resulting α-helix fractions of poly-L-glutamic acid at pH 4.3 calculated from the UVRR spectra. Adapted from ref 54.

Excitation at ~200 nm gives rise to strong UVRR spectra that show particular peptide bond vibrations,[49] that include the amide I (AmI) vibration (~1660 cm^{-1}) that consists mainly of C═O stretching and a small amount of out-of-phase C—N stretching, the amide II (AmII) vibration (~1550 cm^{-1}) that consists of an out-of-phase combination of C—N stretching and N—H bending motions, and the amide III (AmIII) vibration (between ~1200 and 1340 cm^{-1}), which is a complex vibration involving C—N stretching and N—H bending. A vibration that contains significant C_α—H bending (~1390 cm^{-1}) is also enhanced if the peptide bond conformation causes the coupling of C_α—H bending to C—N stretching and N—H bending.

These UVRR-enhanced peptide bond vibrations (except for the AmI) derive from local modes within individual peptide bonds. The AmI vibrations show small couplings between adjacent peptide bonds.[50,51] The local mode character of the AmII, AmIII, and C_α—H bending peptide bond vibrations allows the measured UVRR spectrum to be modeled as the linear sum of contributions of the individual peptide bond UVRR spectra.[52]

This enabled Asher and co-workers to develop a quantitative methodology to determine protein secondary structure directly from the measured UVRR spectra.[53] They measured the UVRR spectra of a set of proteins with known X-ray structures and determined the "basis" spectra of the three major secondary structure motifs, the α-helix, β-sheet, and unfolded conformations. These basis spectra represent the average pure secondary structure Raman spectra (PSSRS) of α-helix, β-sheet, and unfolded conformations.[53] The fractional secondary structure composition of a protein with an unknown secondary structure can be uniquely determined by linearly fitting the PSSRS to the protein UVRR spectra. The fitted weighting fractions are the fractional amounts of each secondary structure motif.[53]

Correlation between Spectral Features and Protein Secondary Structure. The UVRR spectra of proteins and peptides are conformationally sensitive, as shown in the Figure 2 UVRR study of α-helix melting of poly-L-glutamic acid (PGA) at pH 4.3. PGA is α-helical at low temperatures but melts to unfolded structures at high temperatures.[54] The α-helix low-temperature UVRR spectrum shows an AmI band at ~1660 cm^{-1}, an AmII band at ~1560 cm^{-1}, and an AmIII band centered around 1300 cm^{-1}. As the temperature increases, the AmI band upshifts from ~1660 to ~1670 cm^{-1} and becomes broader, while the AmII band downshifts from ~1560 to ~1555 cm^{-1}. These results indicate weakened hydrogen bonding (HB) with increasing temperature. Previous work showed that water HB to the peptide bond C═O site increases the C═O bond length and, thus, downshifts the AmI band, while water HB to the peptide bond N—H upshifts the AmII band. Thus, the extent of HB partially determines the UVRR band frequencies. The C_α—H intensity increase with temperature indicates α-helix melting.[53,55] The α-helix conformation shows a negligible C_α—H bending band intensity, in contrast to the unfolded extended conformation that has a high C_α—H bending intensity.[53,55]

The AmIII region contains three sub-bands, $AmIII_1$, $AmIII_2$, and $AmIII_3$. However, only two of these sub-bands are clearly resolved in the AmIII region of PGA, the $AmIII_2$ band (~1303 cm^{-1}) and the $AmIII_3$ band (~1250 cm^{-1}). The $AmIII_3$ band, which is most sensitive to conformation, derives from motions that involve coupling of N—H bending to C_α—H bending and C—N stretching.[56,57] As the temperature increases, the concentration of melted polyproline II (PPII)-like conformation increases, and the corresponding unfolded PPII $AmIII_3$ band (~1247 cm^{-1}) in PGA becomes more prominent, overshadowing the low-temperature α-helical $AmIII_3$ band. This clearly signals melting of the α-helix conformation to a PPII conformation.

The large $AmIII_3$ band frequency conformational dependence derives from the fact that coupling between C_α—H bending and N—H bending peptide bond motion depends sensitively on the peptide bond Ramachandran Ψ dihedral angle that, in part, defines the peptide bond secondary structure conformation.[57]

Determination of Psi (Ψ) Angle Distribution. The Asher group discovered a sinusoidal dependence of the $AmIII_3$ frequency on this Ramachandran Ψ angle.[54] Conveniently, they also found little dependence of the $AmIII_3$ frequency on the other dihedral angle, the Ramachandran Φ angle (for sterically allowed Ψ angles).[56] The origin of this Ψ angle frequency difference between the α-helix and extended conformations results from the fact that the α-helix peptide bond conformations have trans N—H and C_α—H bonds that prevent coupling (Figure 3). Thus, the α-helix $AmIII_3$ frequency occurs at 1258 cm^{-1}, and the C_α—H band contains negligible C—N and N—H bending motion and is, thus, not resonance-enhanced.

In contrast, peptide bonds adopting an extended PPII-like conformation have cis N—H and C_α—H bonds whose motions couple well. The $AmIII_3$ band frequency downshifts to 1245 cm^{-1}, and the C_α—H bending vibration contains C—N stretching and N—H bending motions, resulting in resonance enhancement.[54] Quantitative relations were developed to relate the $AmIII_3$ band frequencies to Ramachandran Ψ angles for different peptide bond HB states,[57] for example, for peptide bonds fully hydrogen bonded to water, such as in PPII, 2.5_1-helix, and extended β-strand conformations

$$\nu^{EXT}_{AmIII_3}(\Psi, T) = 1256\ cm^{-1} - 54\ cm^{-1}\cdot\sin(\Psi + 26°) - 0.11\ (cm^{-1}/°C)T \quad (1)$$

where T is the temperature.

DOI: 10.1021/jz101619f | J. Phys. Chem. Lett. 2011, 2, 334–344

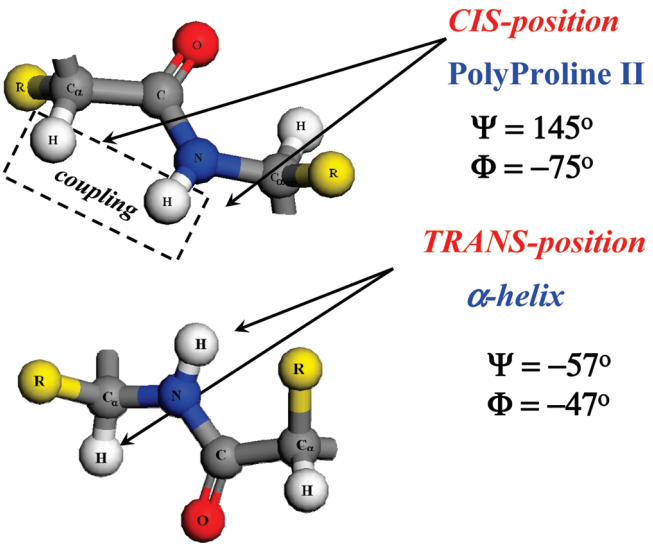

Figure 3. Relative orientations of N—H and C_α—H bonds in the polyproline II and α-helix conformations.

The family of quantitative relationships determining the $AmIII_3$ frequencies ignore the more modest Ramachandran Φ angle dependencies.[56] Equations have been proposed to allow estimation of the Ψ angle for the different possible peptide bond HB states. The estimated error of this determination is suggested to be ≤±14°.[57] Figure 4 shows the family of theoretical curves that correlate the $AmIII_3$ frequencies to the Ramachandran Ψ angles for the different HB states.[57] As shown below, correlating the inhomogeneously broadened $AmIII_3$ band shape to the underlying Ramachandran Ψ angle distribution enables the determination of the peptide bond conformational distribution in peptides and proteins. Most importantly, this conformational distribution can be used to calculate the Gibbs free-energy landscape along the Ψ angle coordinate, which is the most important (un)folding reaction coordinate.

The UVRR spectra show inhomogeneously broadened Raman bands that reflect the distribution of conformations experienced by the protein. In the case of the $AmIII_3$ band, the inhomogeneous distribution reflects mainly the distribution of peptide bond Ψ angles and HB states.

The UVRR spectra show inhomogeneously broadened Raman bands that reflect the distribution of conformations experienced by the protein.

We assume that the experimentally measured, inhomogeneously broadened $AmIII_3$ band, $A(\nu)$, derives from the sum of M Lorentzian bands which result from the different peptide bond conformations with different band frequencies, νe_i. The $AmIII_3$ band homogeneous line width, $\Gamma = 7.5\ cm^{-1}$,

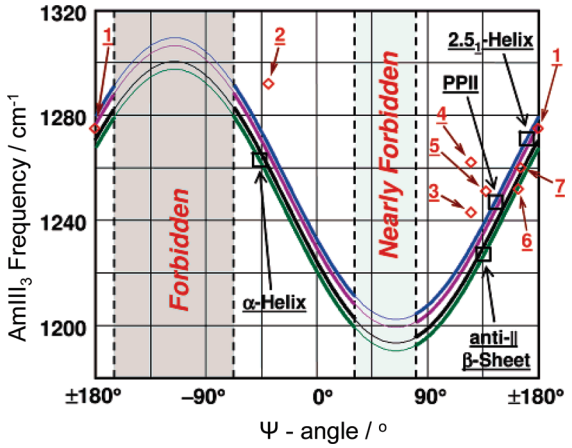

Figure 4. Correlation between $AmIII_3$ frequency, peptide bond HB pattern, and Ramachandran Ψ angle; (□) measured $AmIII_3$ frequencies of α-helix, antiparallel β-sheet, PPII, and 2.5_1-helix in aqueous solution; (◇) measured $AmIII_3$ frequencies of peptide crystals, plotted against their Ψ angles (1) Ala-Asp, (2) Gly-Ala-Leu·$3H_2O$, (3) Val-Glu, (4) Ala-Ser, (5) Val-Lys, (6) Ser-Ala, and (7) Ala-Ala. The blue curve is the predicted correlation (eq 1) for full HB to water (PPII, 2.5_1-helix, and extended β-strand); the green curve is a theoretically predicted correlation (eq 1) for two end-on peptide bond−peptide bond HBs (α-helix-like conformation and interior strands of β-sheet); the magenta curve is the predicted correlation (eq 1) for the peptide bond where only the C═O group has a peptide bond−peptide bond HB (three α-helix N-terminal peptide bonds and half of the peptide bonds of the exterior strands of the β-sheet); the black curve is the predicted correlation (eq 1) for the peptide bond with just the N—H group peptide bond−peptide bond HB (three α-helix C-terminal peptide bond and the other half of the peptide bond of the exterior strand of the β-sheet). Reproduced from ref 57.

was determined from UVRR measurements of small peptide crystals in defined secondary structure states[58]

$$A(\nu) = \pi^{-1} \sum_{i=1}^{M} L_i \frac{\Gamma^2}{(\nu - \nu e_i)^2 + \Gamma^2} \qquad (2)$$

where L_i is the probability for the contributing band to occur at frequency νe_i.

We can deconvolute out the homogeneous line width from the peptide bond UVRR spectra to calculate the underlying inhomogeneously broadened $AmIII_3$ band shape,[58] leading to the calculation of the frequency distribution of the $AmIII_3$ band. We can then use eq 1, relating the $AmIII_3$ band frequency to the Ramachandran Ψ angle, to convert the frequency distributions to Ψ angle distributions (Figure 5). Figure 5A shows histogram plots of the calculated underlying $AmIII_3$ band frequency distributions for a set of peptides and proteins. The XAO peptide of sequence Ac-XXAAAAAAAOO-NH_2 (A is alanine, O is ornithine, X is diaminobutyric acid) is known to be primarily in a PPII conformation.[59] As shown in Figure 5A, the XAO frequency distribution is similar to that of Ala_5-Ala_3 (the difference UVRR between Ala_5 and Ala_3 that models the spectrum of the interior Ala_5 peptide bonds). This result indicates that these peptide bonds predominantly populate the PPII conformation, as do the peptide bonds of a 21-residue mainly alanine peptide (AP) of sequence AAAAA(AAARA)$_3$A at elevated temperature. Acid-denatured apomyoglobin shows a broad frequency distribution, as expected, from its broad

DOI: 10.1021/jz101619f | J. Phys. Chem. Lett. 2011, 2, 334–344

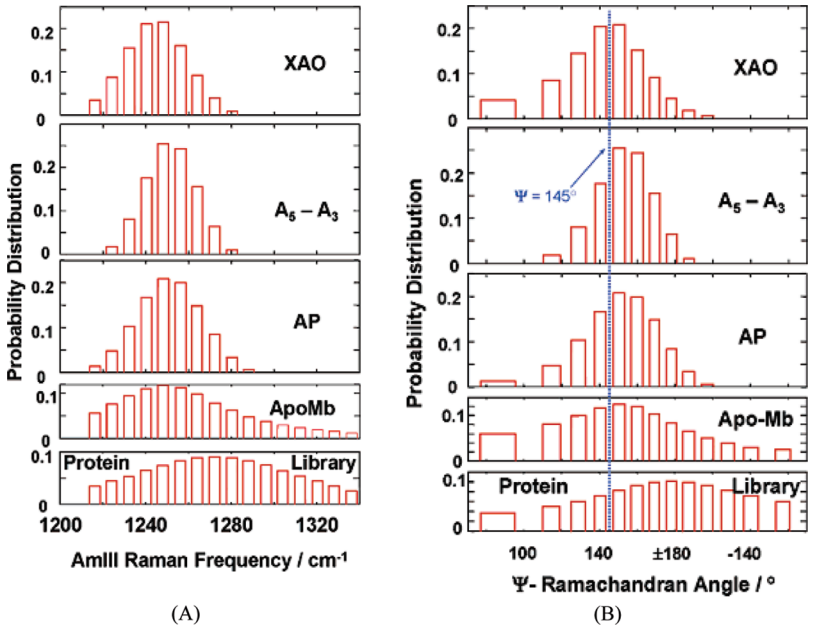

Figure 5. (A) Frequency distribution of the $AmIII_3$ band calculated by deconvolution of homogenously broadened $AmIII_3$ band profiles of XAO of the sequence Ac-XXAAAAAAAOO-NH_2 (A is alanine, O is ornithine, X is diaminobutyric acid), A_5-A_3 (Ala_5-Ala_3), non-α-helical AP of the sequence AAAAA-$(AAARA)_3$A, acid-denatured apomyoglobin, and "disordered" protein conformations. The resulting histogram shows the population distribution underlying the measured $AmIII_3$ band. (B) Estimated Ramachandran Ψ angle distribution of XAO, A_5-A_3, non-α-helical AP, acid-denatured apomyoglobin, and "disordered" protein conformations. Reproduced from ref 58.

distribution of conformations. The "protein library", of course, shows the broadest frequency distribution. Figure 5B shows the calculated Ramachandran Ψ angle distributions for the samples. These plots are obtained by converting the frequency distributions of Figure 5A into Ramachandran Ψ angle distributions using eq 1.

Further, by applying the Boltzmann relation to the Ψ angle distributions, we can calculate the relative Gibbs free energy along the Ramachandran Ψ angle coordinate because the population at any particular Ψ angle is determined by its relative Gibbs free energy.[58]

For example, this approach was used to determine the Gibbs free-energy landscape for poly-L-lysine (PLL). At neutral and low pH values, PLL adopts extended conformations that includes the PPII and 2.51-helix conformations. The 2.51-helix conformation results from the PLL charged side chains' electrostatic repulsions.[60] Ma et al.[55] used UVRR to monitor the temperature and $NaClO_4$ concentration dependence of the PLL Gibbs free-energy landscape (Figure 6). They observed an α-helix-like basin containing α-helix and π-bulge conformations and a basin containing PPII and 2.51-helical extended conformations.

As indicated in Figure 6, adding $NaClO_4$ induces a change from a solution equilibrium between extended PPII and 2.51-helical conformations to an equilibrium involving α-helix-like conformations. This conformational change results from charge screening due to strong ion-pair formation between ClO_4^- and the lysine side chain $—NH_3^+$ that reduces the repulsion between charged side chains. Figure 6 also shows that increasing temperatures cause the α-helix-like conformations to melt to extended conformations.

T-Jump Kinetic Studies of Protein Folding. Dynamic UVRR measurements can be used to elucidate biomolecular structural dynamics.[61,62] UVRR *T*-jump measurements can elucidate the evolution of peptide and protein secondary structure.[61−70] These studies probe the evolution between different secondary structural motifs such as α-helix, 3_{10}-helix, π-bulge, and PPII conformations.[71] The rates of these transitions occur in the 100 ns to ∼2 μs time regime.

Recent nanosecond to microsecond protein folding dynamics studies find complex unfolding behaviors. For example, recent studies of the mainly alanine peptide (AP) melting demonstrate a complex pathway that involves melting of multiple α-helix-like structures, which include the 3_{10}-helix, π-bulge, and pure α-helix conformations that have different melting curves than the PPII-like unfolded conformation.[63]

To gain insight into the dynamics of protein (un)folding, the Asher group constructed the first *T*-jump UVRR spectrometer that they used to examine conformational relaxation subsequent to nanosecond *T*-jumps.[61−63] The peptide and protein relaxation after the *T*-jump utilizes folding and unfolding conformational change coordinates that are easily studied with UVRR. These *T*-jumps used ∼5 ns excitation pulses at 1.9 μm that occur within a water vibrational overtone absorption band. Thermalization of the absorbed energy occurs within 70 ps.[72,73] It is easy to achieve ∼20 °C *T*-jumps from the ∼5 ns IR laser pulses.

In their first kinetic studies, the Asher group examined the kinetics of melting of the AP that is mainly α-helical at low temperature.[63] Steady-state measurements showed that the α-helix melts to a PPII conformation. Figure 7A shows the *T*-jump relaxation transient difference UVRR spectra of AP in H_2O and D_2O. The transient difference spectra measured at delay times as long as 1 μs were modeled using a linear combination of α-helix and the PPII equilibrium UVRR basis

DOI: 10.1021/jz101619f | J. Phys. Chem. Lett. 2011, 2, 334–344

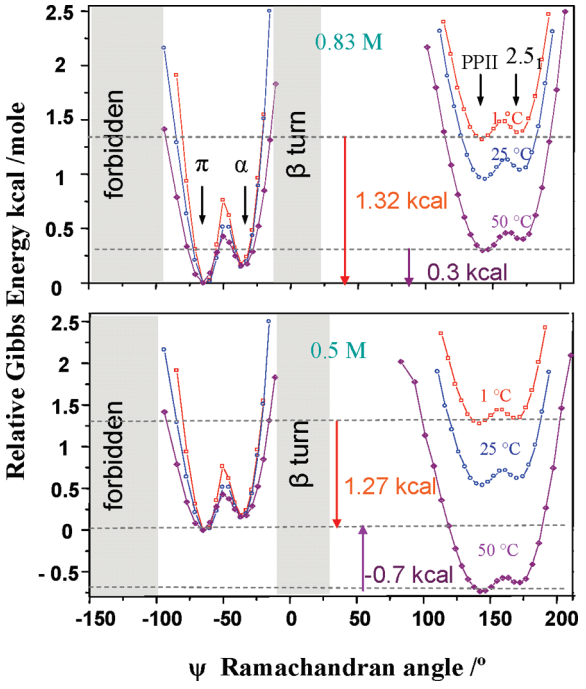

Figure 6. Estimated Gibbs free-energy landscape for poly-L-lysine in 0.83 and 0.5 M $NaClO_4$ at 1, 25, and 50 °C. Increasing the $NaClO_4$ concentration from 0.5 to 0.83 M stabilizes the α-helix-like conformation. Increased temperatures stabilize the unfolded conformations. Adapted from ref 55.

spectra. The first spectral changes evident at < 10 ns derive from fast HB changes of water bound to the peptide bonds in the PPII state due to the temperature increase.[61,62]

Subsequent relaxation spectral changes result from peptide bond conformation changes. Modeling of the transient spectra can determine the kinetics of the AP structural relaxation. Depending on the initial temperature, unfolding time constants between 180 and 240 ns were observed. By assuming a two-state model they calculated a folding time constant of ~1 μs (Figure 7).[61−63]

They also observed a puzzling peculiarity in the temperature dependence of the folding and unfolding rate constants that they calculated from the relaxation rates by assuming a two-state system (that was fully consistent with the observed single-exponential relaxation behavior). As the temperature increased, they calculated that the folding rate constant decreased, indicating a negative activation energy of -4^{+3}_{-2} kcal/mol, which indicates an anti-Arrhenius behavior.[62,63] Obviously, this peculiarity must result from the fact that the conformational transition is not two-state.

Subsequently, Mikhonin et al. identified the additional states involved in the melting transition.[74] They found that they could spectrally differentiate α-helix-like conformational substates from the $AmIII_3$ band frequency distribution. They calculated the α-helix-like UVRR spectrum by subtracting off the pure PPII UVRR spectrum measured at higher temperature (after accounting for the temperature dependence of the PPII UVRR spectrum). Figure 8A shows the calculated Ramachandran angle distributions in AP between 0 and 30 °C.

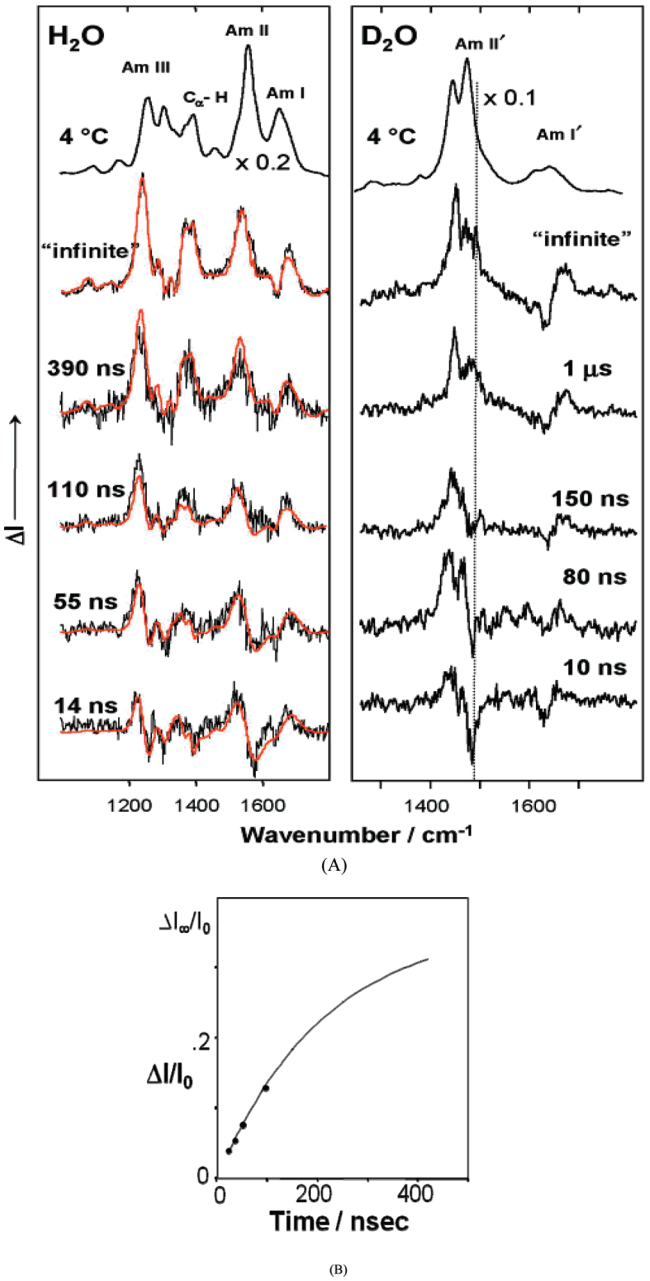

Figure 7. (A) AP UVRR spectra measured in water and D_2O solution at 4 °C (top) and transient difference spectra of AP in solution initially at 4 °C measured at different delay times following a *T*-jump of ~31 °C (~22 °C in D_2O). (B) Kinetics of thermal denaturation of AP. The ordinate axis is the relative change in the UV Raman intensity at 1236 cm^{-1} obtained from the transient difference spectra of Figure 14 of ref 62. The abscissa is the time delay at which the spectra were acquired following the *T*-jump. Reproduced from refs (A) 61 and (B) 62.

At low temperatures, the Ψ angle distribution of the α-helix-like state is broad and spans the Ψ angles of the pure α-helix, 3_{10}-helix, and π-helix bulge conformations. As the temperature increases, the α-helix-like Ψ angle distribution narrows until at 30 °C, the distribution becomes very narrow and centered at −42°, the Ψ angle of the pure α-helix.

DOI: 10.1021/jz101619f | J. Phys. Chem. Lett. 2011, 2, 334–344

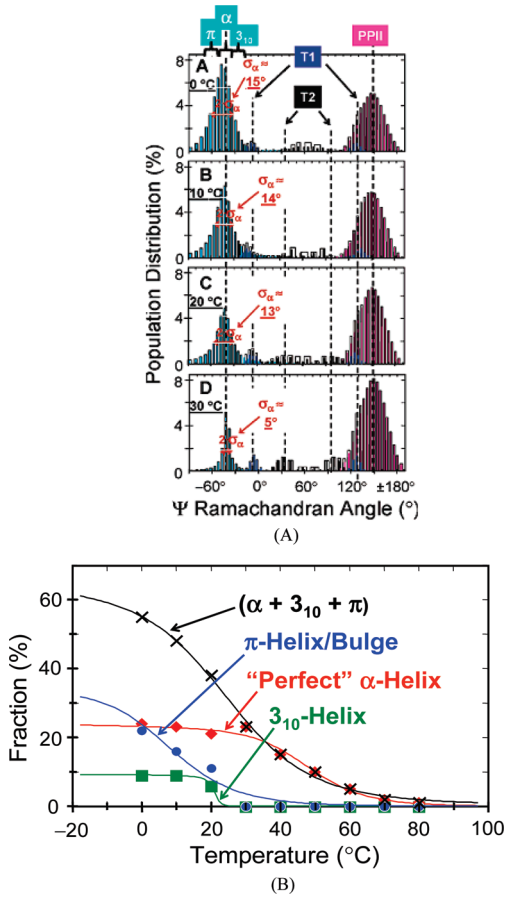

Figure 8. (A) Calculated Ramachandran Ψ probability distributions in AP at (A) 0, (B) 10, (C) 20, and (D) 30 °C. Reproduced from ref 74. (B) Melting curves for AP α-helix-like conformations. (×) Original α-helix melting curve as reported by Lednev et al. (refs 61 and 62), which is a sum of individual α-, π-, and 3_{10}-helical melting curves; (red ♦) pure α-helix melting; (green ■) 3_{10}-helix (type III turn) melting; (blue ●) π-bulge (π-helix) melting. Adapted from ref 74.

Figure 8B shows the melting curves determined for these different α-helix-like conformations by assuming identical Raman cross sections for the pure α-helix, the 3_{10}-helix, and the π-bulge conformations. T_m was determined to be 45, 20 and 10 °C for the α-helix, 3_{10}-helices, and π-bulges, respectively.

The anti-Arrhenius behavior observed by Lednev et al.'s *T*-jump measurements directly results from these different T_m for the 3_{10}-helix, π-bulge, and pure α-helix conformations.[75] As the temperature increases, the pure α-helix conformation increasingly dominates the equilibrium conformational distribution. Apparently, the folding rate of the pure α-helix conformation is slowest. These studies clearly show the utility of UVRR to gain crucial insight into the complex nature of peptide folding dynamics.

These types of *T*-jump studies can give important biological insight. For example, in a recent protein *T*-jump study, Spiro et al.[70] examined the early events in the unfolding of apomyoglobin using both 197 and 229 nm excitation. These excitations allowed them to probe both the aromatic side chains and the peptide backbone conformations. Aromatic amino acid side chain UVRR bands can monitor the solvent exposure, while the peptide bond UVRR bands report on backbone Ramachandran Ψ angles, as discussed above. Measuring both spectral bands can answer the question of whether a changing solvent exposure of the protein core precedes or follows secondary structure changes. The authors were able to clearly differentiate the order of these events. They found that the Trp14 bands respond twice as fast as does the peptide bond α-helix melting. Thus, Trp14 that is originally buried in the protein core becomes exposed to solvent prior to melting of the protein core.

Kinetic IR *T*-jump experiments have also been carried out on α-helical peptides.[22,76] For instance, in their IR studies, the Dyer group found that suc-F_s 21-peptide (a peptide very similar to AP) shows fast unfolding kinetics with a time constant of ∼160 ns.[22] This result is consistent with the UVRR studies of Lednev et al.[63] In another IR *T*-jump kinetic study, the Gai group examined the helix−coil transition of an α-helical peptide and its deuterated analogue, Ac-YGSPEA$_3$KA$_4$KA$_4$-CO-D-Arg-CONH$_2$ and Ac-YGSPEA$_3$KAAAAKA$_4$-CO-D-Arg-CONH$_2$, where the underlined residues are ^{13}C-labeled. This design was meant to use the ^{13}C═O AmI band of the central Ala residues to probe conformational changes associated with only the middle of the peptide sequence and to discriminate it from signals due to end-fraying. They reported a complex helix−coil transition that does show single-exponential relaxation.[76] Their multiexponential relaxation kinetics based on ^{13}C═O AmI band changes show a component with a time constant of 230 ns similar to ours that does not arise from end-fraying.[22,63] The IR peptide folding dynamic studies show less information content because they only monitor the AmI band,[22,76] whereas UVRR monitors the $C_α$—H, AmII and AmIII bands, in addition to the AmI band. Thus, UVRR can give a more informative picture of peptide folding dynamics. Further, as shown in Figure 2, the spectral dependence of the AmI band is less than that for the AmIII$_3$ and the $C_α$—H bending bands.

Other UVRR Insights. A number of other recent UVRR studies have also illustrated the important protein information available. For example, Ianoul et al. used UVRR to examine the peptide backbone spatial dependence of α-helix melting of deuterium-labeled AP (AdP).[71] In AdP, all of the Ala residues except the four central ones were selectively deuterated. They found that melting of the isotopically labeled exterior peptide bonds could be spectrally resolved from the central ones, thus allowing the spatial resolution of the peptide bond conformational changes. The results show that the central residues are essentially 100% α-helix-like at 0 °C with a T_m of 32 °C, while the exterior residues are ∼60% α-helix-like at 0 °C with a T_m of 5 °C.

More recently, Lednev's group reported the application of UVRR for studying amyloid fibrils,[77,78] which are well-organized protein aggregates associated with many neurodegenerative diseases. Amyloid fibrils are not soluble and do not form crystals, limiting the application of conventional NMR spectroscopy and X-ray crystallography, two major biophysical tools of structural biology. UVRR spectroscopy is uniquely suitable for characterizing the protein structure at all stages of fibrillation. Chemometric[79] and 2D correlation[80] analysis of UVRR spectra allowed for direct monitoring of the fibrillation

DOI: 10.1021/jz101619f | *J. Phys. Chem. Lett.* 2011, *2*, 334–344

nucleus,[81] establishing the sequential order of changes in the protein secondary structure and the kinetic mechanism of lysozyme fibrillation.[82]

Their combination of hydrogen−deuterium exchange with UVRR and advanced statistics enabled them to determine the spectroscopic signature of the fibril core.[83] They then utilized our method described above to determine the Ramachandran Ψ angle distribution in the fibril core.[84,85] This information is a powerful constraint for determining the conformation of β-strands in the fibril core. This approach is the only experimental tool available at the moment to directly characterize the cross-β core structure in fibrils prepared from the full-length proteins. X-ray crystallography of small peptide microcrystals mimicking the fibril core and solid-state NMR of fibrils, prepared from isotope-labeled peptides, can provide the atomic-resolution structure of the fibril core. UVRR−hydrogen−deuterium exchange indicated a significant variability in the core structure of fibrils prepared from different proteins.[84,85] In addition, it allowed differentiation of parallel and antiparallel β-sheets in the cross-β core of amyloid β fibrils.[84] Moreover, the conformation of the parallel β-sheet in the $A\beta_{1-40}$ fibril core was atypical for globular proteins, while, in contrast, the antiparallel β-sheet in $A\beta_{32-42}$ fibrils was a common structure in globular proteins.[84] Consistent with the latter observation, the Raman signature of the fibrillar-type β-sheet was required in addition to the globular protein β-sheet to satisfactorily fit the UVRR spectra of the aggregated prion protein.[86]

Future Direction and Outlook. The UVRR methodologies discussed in this Perspective enable incisive investigations into the mechanism of protein folding. Future studies will include single peptide bond conformational changes and studies of the conformation of side chains such as Phe, Tyr, Trp, Arg, Asn, and Gln.

Resolution of Individual Peptide Bond Conformational Changes. The current state-of-the-art UVRR measurements lack sufficient S/N to monitor conformational changes at the single peptide bond level of a ∼100 residue protein. However, UVRR instrumentation continues to advance due to improvements in laser technology and the development of UV Raman spectrometers with dramatically improved spectral dispersion that enable dramatically increased throughput. We are constructing a spectrometer which utilizes very high dispersion gratings with optics specially coated for deep UV efficiencies. The increased S/N will enable the monitoring of the Gibbs free-energy landscape of individual peptide bonds in a peptide or protein. C_α deuteration silences the Ψ angle dependence of the $AmIII_3$ band frequency. Thus, the difference UVRR between a C_α deuterium-labeled and the natural abundance protein reveals the $AmIII_3$ band of the labeled peptide bond; the frequencies and band shapes reveal its Ramachandran Ψ angle distribution, which reveals its Gibbs free-energy landscape. *T*-jump kinetic measurements of the isotope-labeled difference spectra will reveal the individual peptide bonds' activation barriers that control (un)folding mechanisms.

Amino Acid Side Chain Conformations. There are numerous amino acid side chain chromophores that show UVRR-enhanced bands with ∼200 nm UVRR excitation. These UVRR bands can be used to monitor amino acid side chain conformations and their interactions with other side chains and the backbone peptide bonds. There is now a deep understanding of the conformational dependence of the Trp, Tyr, and Phe aromatic amino acid UVRR spectra.[87,88] In contrast, there are few studies of the UVRR bands of these residues[89] and no published studies, to our knowledge, of Arg, Asn, and Gln residues. The Asn and Gln side chains give rise to UVRR-enhanced primary amide UVRR bands that partially overlap the peptide bond amide bands. These can be selectively monitored by comparing very deep UV, ∼195 nm UVRR, for example, to UVRR spectra excited at 204 nm; primary amides show their $\pi \rightarrow \pi^*$ transition at shorter wavelengths than the peptide bond $\pi \rightarrow \pi^*$ transition.[90] Thus, appropriately scaled 195−204 nm difference spectra will display the side chain primary amide bands.

We are now characterizing the UVRR spectra of Asn and Gln side chain vibrations in order to determine their HB dependence. This will ultimately enable UVRR to detect HB of side chains in peptides and proteins. The Arg side chain shows an isolated band at 1178 cm^{-1}, which is easily observed in AP, for example.[46] Our work is also investigating the role of Arg residues in α-helix stabilization.

The unique utility of UVRR for the study of protein folding is discussed in this Perspective. Specifically, we have shown how peptide bond resonance Raman enhancement permits the study of protein secondary structure by using ∼200 nm UV excitation. It now is clear that UVRR is the most useful dilute solution method to quickly determine protein and peptide secondary structure. The sinusoidal dependence of the $AmIII_3$ Raman band frequency on the Ramachandran Ψ angle enables the determination of solution peptide bond Ψ angle distributions. The measurement of this distribution reveals the Gibbs free-energy landscape along the Ψ angle protein (un)folding coordinate. Kinetic *T*-jump studies allow the examination of the kinetics of protein folding and reveal aspects of the activation barriers between equilibrium conformations. The application of UVRR to the study of the formation mechanism of amyloid fibrils is an important illustration of the power of the technique to probe structure and dynamics. The development of statistical methods for the analysis of UVRR spectra dramatically increases the information content of the spectroscopy.

The increased S/N will enable the monitoring of the Gibbs free-energy landscape of individual peptide bonds in a peptide or protein.

UVRR is the most useful dilute solution method to quickly determine protein and peptide secondary structure.

DOI: 10.1021/jz101619f | *J. Phys. Chem. Lett.* 2011, *2*, 334–344

AUTHOR INFORMATION

Corresponding Author:

*To whom correspondence should be addressed. E-mail: asher@pitt.edu. Phone: 412-624-8570. Fax: 412-624-0588.

Biographies

Sulayman Oladepo received his Ph.D. from the University of Alberta, under the supervision of Prof. Glen Loppnow. He is currently doing his postdoctoral work in the laboratory of Prof. Sanford Asher at the University of Pittsburgh. His current research involves the use of UV resonance Raman spectroscopy to study the melting dynamics of β-sheet structures and the effects of citrullination on protein folding dynamics.

Kan Xiong received his Bachelor's Degree in Chemistry from the University of Science and Technology of China in 2006. He is currently a senior graduate student under the direction of Prof. Sanford A. Asher at the University of Pittsburgh and is working on using UV resonance Raman spectroscopy to study protein and peptide folding.

Zhenmin Hong is currently a graduate student in the Department of Chemistry, University of Pittsburgh. He received B.S. and M.S. degrees from Tsinghua University, China. His research interest includes using UV resonance Raman spectroscopy to study protein and peptide structure and folding. He is now examining the effect of side chain interactions on determining peptide conformations.

Sanford Asher is Distinguished Professor of Chemistry at the University of Pittsburgh. He received his Bachelor's degree from the University of Missouri at St. Louis in 1971 and his Ph.D. in 1977 from UC Berkeley. Following postdoctoral work in Applied Physics at Harvard, he joined the department of Chemistry of the University of Pittsburgh in 1980. His current research concentrates on developing UV resonance Raman spectroscopy for probing protein structure and dynamics. His research group also investigates and develops photonic crystal materials and sensors. See http://www.pitt.edu/~asher/homepage/index.html

ACKNOWLEDGMENT The authors gratefully thank Igor Lednev for helping us describe his groups fibrillation studies. We also gratefully acknowledge NIH Grant 1R01EB009089 for funding.

REFERENCES

(1) Baldwin, R. L.; Rose, G. D. Is Protein Folding Hierarchic? I. Local Structure and Peptide Folding. *Trends Biochem. Sci.* **1999,** *24*, 26–33.

(2) Baldwin, R. L.; Rose, G. D. Is Protein Folding Hierarchic? II. Folding Intermediates and Transition States. *Trends Biochem. Sci.* **1999,** *24*, 77–83.

(3) Dobson, C. M. The Structural Basis of Protein Folding and Its Links with Human Disease. *Philos. Trans. R. Soc. London, Ser. B* **2001,** *356*, 133–145.

(4) Dobson, C. M.; Sali, A.; Karplus, M. Protein Folding: A Perspective from Theory and Experiment. *Angew. Chem., Int. Ed.* **1998,** *37*, 868–893.

(5) Jahn, T. R.; Radford, S. E. The Yin and Yang of Protein Folding. *FEBS* **2005,** *272*, 5962–5970.

(6) Lindberg, M. O.; Oliveberg, M. Malleability of Protein Folding Pathways: A Simple Reason for Complex Behaviour. *Curr. Opin. Struct. Biol.* **2007,** *17*, 21–29.

(7) Daggett, V.; Fersht, A. The Present View of the Mechanism of Protein Folding. *Nat. Rev. Mol. Cell Biol.* **2003,** *4*, 497–502.

(8) Anfinsen, C. B.; Haber, E.; Sela, M.; White, F. H., Jr. The Kinetics of Formation of Native Ribonuclease During Oxidation of the Reduced Polypeptide Chain. *Proc. Natl. Acad. Sci. U.S.A.* **1961,** *47*, 1309–1314.

(9) Matthews, C. R. Pathways of Protein-Folding. *Annu. Rev. Biochem.* **1993,** *62*, 653–683.

(10) Thirumalai, D.; Woodson, S. A. Kinetics of Folding of Proteins and RNA. *Acc. Chem. Res.* **1996,** *29*, 433–439.

(11) Kim, P. S.; Baldwin, R. L. Specific Intermediates in the Folding Reactions of Small Proteins and the Mechanism of Protein Folding. *Annu. Rev. Biochem.* **1982,** *51*, 459–489.

(12) Karplus, M.; Weaver, D. L. Protein Folding Dynamics. *Nature* **1976,** *260*, 404–406.

(13) Daggett, V.; Fersht, A. R. Is There a Unifying Mechanism for Protein Folding? *Trends Biochem. Sci.* **2003,** *28*, 18–25.

(14) Dill, K. A.; Chan, H. S. From Levinthal to Pathways to Funnels. *Nat. Struct. Biol.* **1997,** *4*, 10–19.

(15) Mello, C. C.; Barrick, D. An Experimentally Determined Protein Folding Energy Landscape. *Proc. Natl. Acad. Sci. U.S.A.* **2004,** *101*, 14102–14107.

(16) MacKerell, A. D., Jr.; Bashford, D.; Bellott, M.; Dunbrack, R. L., Jr.; Evanseck, J. D.; Field, M. J.; Fischer, S.; Gao, J.; Guo, H.; Ha, S.; et al. All-Atom Empirical Potential for Molecular Modeling and Dynamics Studies of Proteins. *J. Phys. Chem. B* **1998,** *102*, 3586–3616.

(17) Cantor, C. R.; Schimmel, P. R. Absorption Spectroscopy. In *Biophysical Chemistry*; McCombs, L. W., Ed.; W. H. Freeman and Company: San Francisco, CA, 1980; Vol. 2, pp 349−408.

(18) Rosenheck, K.; Doty, P. The Far Ultraviolet Absorption Spectra of Polypeptide and Protein Solutions and Their Dependence on Conformation. *Proc. Natl. Acad. Sci. U.S.A.* **1961,** *47*, 1775–1785.

(19) Kallenbach, N. R.; Lyu, P.; Zhou, H. CD Spectroscopy and the Helix-Coil Transition in Peptides and Polypeptides. In *Circular Dichroism and Conformational Analysis of Biomolecules*; Fasman, G. D., Ed.; Plenum Press: New York, 1996; pp 201−259.

(20) Mittermaier, A.; Kay, L. E. Review — New Tools Provide New Insights in NMR Studies of Protein Dynamics. *Science* **2006,** *312*, 224–228.

(21) Wuthrich, K. NMR — This Other Method for Protein and Nucleic-Acid Structure Determination. *Acta Crystallogr., Sect. D* **1995,** *51*, 249–270.

(22) Williams, S.; Causgrove, T. P.; Gilmanshin, R.; Fang, K. S.; Callender, R. H.; Woodruff, W. H.; Dyer, R. B. Fast Events in Protein Folding: Helix Melting and Formation in a Small Peptide. *Biochemistry* **1996,** *35*, 691–697.

(23) Hendra, P. J. Sampling Consideration for Raman Cpectroscopy. In *Handbook of Vibrational Spectroscopy*; Chalmers, J. P., Griffiths, P. R., Eds.; John Wiley & Sons: London, 2002; Vol. 2, pp 1263−1288.

(24) Everall, N. J. Raman Spectroscopy of the Condensed Phase. In *Handbook of Vibrational Spectroscopy*; Chalmers, J. P., Griffiths, P. R., Eds.; John Wiley & Sons: London, 2002; Vol. 1, pp 141−148.

(25) Weber, A. Raman Spectroscopy of Gases. In *Handbook of Vibrational Spectroscopy*; Chalmers, J. P., Griffiths, P. R., Eds.; John Wiley & Sons: London, 2002; Vol. 1, pp 176−194.

(26) Long, D. A. *The Raman Effect: A Unified Treatment of the Theory of Raman Scattering by Molecules*; John Wiley & Sons Ltd.: West Sussex, England, 2002.

(27) Kramers, H.; Heisenberg, W. Uber die Streuung von Strahlung durch Atome. *Z. Phys. A: Hadrons Nucl.* **1925,** *31*, 681–708.

(28) Dirac, P. A. M. The Quantum Theory of Dispersion. *Proc. R. Soc. London, Ser. A* **1927,** *114*, 710–728.

(29) Placzek, G. Rayleigh and Raman Scattering. In *Handbuch der Radiologie*; Marx, E., Ed.; Aeademische: Leipzig, Germany, 1934; Vol. 6, p 205.

DOI: 10.1021/jz101619f | *J. Phys. Chem. Lett.* **2011,** *2*, 334–344

(30) Albrecht, A. C. On the Theory of Raman Intensities. *J. Chem. Phys.* **1961,** *34*, 1476–1484.
(31) Lee, S.-Y.; Heller, E. J. Time-Dependent Theory of Raman Scattering. *J. Chem. Phys.* **1979,** *71*, 4777–4788.
(32) Tannor, D. J.; Heller, E. J. Polyatomic Raman Scattering for General Harmonic Potentials. *J. Chem. Phys.* **1982,** *77*, 202–218.
(33) Heller, E. J.; Sundberg, R.; Tannor, D. Simple Aspects of Raman Scattering. *J. Phys. Chem.* **1982,** *86*, 1822–1833.
(34) Asher, S. A. UV Resonance Raman Studies of Molecular Structure and Dynamics: Applications in Physical and Biophysical Chemistry. *Annu. Rev. Phys. Chem.* **1988,** *39*, 537–588.
(35) Myers, A. B. `Time-Dependent' Resonance Raman Theory. *J. Raman Spectrosc.* **1997,** *28*, 389–401.
(36) Asher, S. A. UV resonance Raman-Spectroscopy for Analytical, Physical, and Biophysical Chemistry. 1. *Anal. Chem.* **1993,** *65*, A59–A66.
(37) Asher, S. A. UV resonance Raman-Spectroscopy for Analytical, Physical, and Biophysical Chemistry. 2. *Anal. Chem.* **1993,** *65*, A201–A210.
(38) Palaniappan, V.; Bocian, D. F. Acid-Induced Transformations of Myoglobin. Characterization of a New Equilibrium Heme-Pocket Intermediate. *Biochemistry* **1994,** *33*, 14264–14274.
(39) Chi, Z. H.; Asher, S. A. UV Resonance Raman Determination of Protein Acid Denaturation: Selective Unfolding of Helical Segments of Horse Myoglobin. *Biochemistry* **1998,** *37*, 2865–2872.
(40) Balakrishnan, G.; Hu, Y.; Oyerinde, O. F.; Su, J.; Groves, J. T.; Spiro, T. G. A Conformational Switch to β-Sheet Structure in Cytochrome C Leads to Heme Exposure. Implications for Cardiolipin Peroxidation and Apoptosis. *J. Am. Chem. Soc.* **2007,** *129*, 504–505.
(41) Ahmed, Z.; Beta, I. A.; Mikhonin, A. V.; Asher, S. A. UV Resonance Raman Thermal Unfolding Study of Trp-Cage Shows That it is Not a Simple Two-State Miniprotein. *J. Am. Chem. Soc.* **2005,** *127*, 10943–10950.
(42) Asher, S. A.; Johnson, C. R. Raman Spectroscopy of a Coal Liquid Shows that Fluorescence Interference is Minimized with Ultraviolet Excitation. *Science* **1984,** *225*, 311–313.
(43) Bykov, S.; Lednev, I.; Ianoul, A.; Mikhonin, A.; Munro, C.; Asher, S. A. Steady-State and Transient Ultraviolet Resonance Raman Spectrometer for the 193−270 nm Spectral Region. *Appl. Spectrosc.* **2005,** *59*, 1541–1552.
(44) Asher, S. A.; Bormett, R. W.; Chen, X. G.; Lemmon, D. H.; Cho, N.; Peterson, P.; Arrigoni, M.; Spinelli, L.; Cannon, J. UV Resonance Raman-Spectroscopy Using a New CW Laser Source — Convenience and Experimental Simplicity. *Appl. Spectrosc.* **1993,** *47*, 628–633.
(45) Zhao, X. J.; Chen, R. P.; Tengroth, C.; Spiro, T. G. Solid-State Tunable kHz Ultraviolet Laser for Raman Applications. *Appl. Spectrosc.* **1999,** *53*, 1200–1205.
(46) Sharma, B.; Bykov, S. V.; Asher, S. A. UV Resonance Raman Investigation of Electronic Transitions in α-Helical and Polyproline II-Like Conformations. *J. Phys. Chem. B* **2008,** *112*, 11762–11769.
(47) Asher, S. A.; Chi, Z. H.; Li, P. S. Resonance Raman Examination of the Two Lowest Amide $\pi\pi^*$ Excited States. *J. Raman Spectrosc.* **1998,** *29*, 927–931.
(48) Chen, X. G.; Asher, S. A.; Schweitzerstenner, R.; Mirkin, N. G.; Krimm, S. UV Raman Determination of the $\pi-\pi^*$ Excited-State Geometry of N-Methylacetamide — Vibrational Enhancement Pattern. *J. Am. Chem. Soc.* **1995,** *117*, 2884–2895.
(49) Myshakina, N. S.; Asher, S. A. Peptide Bond Vibrational Coupling. *J. Phys. Chem. B* **2007,** *111*, 4271–4279.
(50) Mix, G.; Schweitzer-Stenner, R.; Asher, S. A. Uncoupled Adjacent Amide Vibrations in Small Peptides. *J. Am. Chem. Soc.* **2000,** *122*, 9028–9029.
(51) Mikhonin, A. V.; Asher, S. A. Uncoupled Peptide Bond Vibrations in α-Helical and Polyproline II Conformations of Polyalanine Peptides. *J. Phys. Chem. B* **2005,** *109*, 3047–3052.
(52) Bykov, S. V.; Asher, S. A. UV Resonance Raman Elucidation of the Terminal and Internal Peptide Bond Conformations of Crystalline and Solution Oligoglycines. *J. Phys. Chem. Lett.* **2010,** *1*, 269–271.
(53) Chi, Z. H.; Chen, X. G.; Holtz, J. S. W.; Asher, S. A. UV Resonance Raman-Selective Amide Vibrational Enhancement: Quantitative Methodology for Determining Protein Secondary Structure. *Biochemistry* **1998,** *37*, 2854–2864.
(54) Asher, S. A.; Ianoul, A.; Mix, G.; Boyden, M. N.; Karnoup, A.; Diem, M.; Schweitzer-Stenner, R. Dihedral Ψ Angle Dependence of the Amide III Vibration: A Uniquely Sensitive UV Resonance Raman Secondary Structural Probe. *J. Am. Chem. Soc.* **2001,** *123*, 11775–11781.
(55) Ma, L.; Ahmed, Z.; Mikhonin, A. V.; Asher, S. A. UV Resonance Raman Measurements of Poly-L-Lysine's Conformational Energy Landscapes: Dependence on Perchlorate Concentration and Temperature. *J. Phys. Chem. B* **2007,** *111*, 7675–7680.
(56) Ianoul, A.; Boyden, M. N.; Asher, S. A. Dependence of the Peptide Amide III Vibration on the Φ Dihedral Angle. *J. Am. Chem. Soc.* **2001,** *123*, 7433–7434.
(57) Mikhonin, A. V.; Bykov, S. V.; Myshakina, N. S.; Asher, S. A. Peptide Secondary Structure Folding Reaction Coordinate: Correlation Between UV Raman Amide III Frequency, Ψ Ramachandran Angle, and Hydrogen Bonding. *J. Phys. Chem. B* **2006,** *110*, 1928–1943.
(58) Asher, S. A.; Mikhonin, A. V.; Bykov, S. V. UV Raman Demonstrates that α-Helical Polyalanine Peptides Melt to Polyproline II Conformations. *J. Am. Chem. Soc.* **2004,** *126*, 8433–8440.
(59) Shi, Z.; Olson, C.; Rose, G.; Baldwin, R.; Kallenbach, N. Polyproline II Structure in a Sequence of Seven Alanine Residues. *Proc. Natl. Acad. Sci. U.S.A.* **2002,** *99*, 9190–9195.
(60) Mikhonin, A. V.; Myshakina, N. S.; Bykov, S. V.; Asher, S. A. UV Resonance Raman Determination of Polyproline II, Extended 2.5_1-Helix, and β-Sheet Ψ Angle Energy Landscape in Poly-L-Lysine and Poly-L-Glutamic Acid. *J. Am. Chem. Soc.* **2005,** *127*, 7712–7720.
(61) Lednev, I. K.; Karnoup, A. S.; Sparrow, M. C.; Asher, S. A. Transient UV Raman Spectroscopy Finds No Crossing Barrier Between the Peptide α-Helix and Fully Random Coil Conformation. *J. Am. Chem. Soc.* **2001,** *123*, 2388–2392.
(62) Lednev, I. K.; Karnoup, A. S.; Sparrow, M. C.; Asher, S. A. α-Helix Peptide Folding and Unfolding Activation Barriers: A Nanosecond UV Resonance Raman Study. *J. Am. Chem. Soc.* **1999,** *121*, 8074–8086.
(63) Lednev, I. K.; Karnoup, A. S.; Sparrow, M. C.; Asher, S. A. Nanosecond UV Resonance Raman Examination of Initial Steps in α-Helix Secondary Structure Evolution. *J. Am. Chem. Soc.* **1999,** *121*, 4076–4077.
(64) JiJi, R. D.; Balakrishnan, G.; Hu, Y.; Spiro, T. G. Intermediacy of Poly(L-proline) II and β-Strand Conformations in Poly-(L-lysine) β-sheet Formation Probed by Temperature-Jump/UV Resonance Raman Spectroscopy. *Biochemistry* **2006,** *45*, 34–41.
(65) Balakrishnan, G.; Hu, Y.; Bender, G. M.; Getahun, Z.; DeGrado, W. F.; Spiro, T. G. Nanosecond T-Jump Induced Unfolding Kinetics of α-Helical Peptide: A UV Resonance Raman Study. *Biophys. J.* **2005,** *88*, 39A–40A.

DOI: 10.1021/jz101619f | *J. Phys. Chem. Lett.* **2011,** *2*, 334–344

(66) Balakrishnan, G.; Hu, Y.; Bender, G. M.; Getahun, Z.; DeGrado, W. F.; Spiro, T. G. Enthalpic and Entropic Stages in α-Helical Peptide Unfolding, from Laser *T*-Jump/UV Raman Spectroscopy. *J. Am. Chem. Soc.* **2007,** *129*, 12801–12808.

(67) Balakrishnan, G.; Hu, Y.; Case, M. A.; McLendon, G. A.; Spiro, T. G. T-Jump Induced Helix to Coil Transition in GCN4 Derivative, A Model Coiled-Coil System: UV Raman Study. *Biophys. J.* **2004,** *86*, 499A–500A.

(68) Balakrishnan, G.; Hu, Y.; Case, M. A.; Spiro, T. G. Microsecond Melting of a Folding Intermediate in a Coiled-Coil Peptide, Monitored by *T*-Jump/UV Raman Spectroscopy. *J. Phys. Chem. B* **2006,** *110*, 19877–19883.

(69) Balakrishnan, G.; Hu, Y.; Spiro, T. G. Temperature-Jump Apparatus with Raman Detection Based on a Solid-State Tunable (1.80−2.05 μm) kHz Optical Parametric Oscillator Laser. *Appl. Spectrosc.* **2006,** *60*, 347–351.

(70) Huang, C. Y.; Balakrishnan, G.; Spiro, T. G. Early Events in Apomyoglobin Unfolding Probed by Laser *T*-Jump/UV Resonance Raman Spectroscopy. *Biochemistry* **2005,** *44*, 15734–15742.

(71) Ianoul, A.; Mikhonin, A.; Lednev, I. K.; Asher, S. A. UV Resonance Raman Study of the Spatial Dependence of α-Helix Unfolding. *J. Phys. Chem. A* **2002,** *106*, 3621–3624.

(72) Phillips, C. M.; Mizutani, Y.; Hochstrasser, R. M. Ultrafast Thermally-Induced Unfolding of RNase-A. *Proc. Natl. Acad. Sci. U.S.A.* **1995,** *92*, 7292–7296.

(73) Lian, T. L., B.; Kholodenko, Y.; Hochstrasser, M. Energy Flow from Solute to Solvent Probed by Femtosecond IR Spectroscopy: Malchite Green and Heme Protein Solutions. *J. Phys. Chem.* **1994,** *98*, 11648–11656.

(74) Mikhonin, A. V.; Asher, S. A. Direct UV Raman Monitoring of 3_{10}-Helix and π-Bulge Premelting During α-Helix Unfolding. *J. Am. Chem. Soc.* **2006,** *128*, 13789–13795.

(75) Mikhonin, A.; Asher, S.; Bykov, S.; Murza, A. UV Raman Spatially Resolved Melting Dynamics of Isotopically Labeled Polyalanyl Peptide: Slow α-Helix Melting Follows 3_{10}-Helices and π-Bulges Premelting. *J. Phys. Chem. B* **2007,** *111*, 3280–3292.

(76) Huang, C.-Y.; Getahun, Z.; Wang, T.; DeGrado, W. F.; Gai, F. Time-Resolved Infrared Study of the Helix-Coil Transition Using ^{13}C-Labelled Helical Peptides. *J. Am. Chem. Soc.* **2001,** *123*, 12111–12112.

(77) Lednev, I. K.; Shashilov, V.; Xu, M. Ultraviolet Raman Spectroscopy is Uniquely Suitable for Studying Amyloid Diseases. *Curr. Sci.* **2009,** *97*, 180–185.

(78) Xu, M.; Ermolenkov, V. V.; Uversky, V. N.; Lednev, I. K. Hen Egg White Lysozyme Fibrillation: A Deep-UV Resonance Raman Spectroscopic Study. *J. Biophoton.* **2008,** *1*, 215–229.

(79) Shashilov, V. A.; Lednev, I. K. Advanced Statistical And Numerical Methods for Spectroscopic Characterization of Protein Structural Evolution. *Chem. Rev.* **2010,** *110*, 5692–713.

(80) Shashilov, V. A.; Lednev, I. K. Two-Dimensional Correlation Raman Spectroscopy for Characterizing Protein Structure and Dynamics. *J. Raman Spectrosc.* **2009,** *40*, 1749–1758.

(81) Shashilov, V.; Xu, M.; Ermolenkov, V. V.; Fredriksen, L.; Lednev, I. K. Probing a Fibrillation Nucleus Directly by Deep Ultraviolet Raman Spectroscopy. *J. Am. Chem. Soc.* **2007,** *129*, 6972–6973.

(82) Shashilov, V. A.; Lednev, I. K. 2D Correlation Deep UV Resonance Raman Spectroscopy of Early Events of Lysozyme Fibrillation: Kinetic Mechanism and Potential Interpretation Pitfalls. *J. Am. Chem. Soc.* **2008,** *130*, 309–317.

(83) Xu, M.; Shashilov, V.; Lednev, I. K. Probing the Cross-β Core Structure of Amyloid Fibrils by Hydrogen−Deuterium Exchange Deep Ultraviolet Resonance Raman Spectroscopy. *J. Am. Chem. Soc.* **2007,** *129*, 11002–11003.

(84) Popova, L. A.; Kodali, R.; Wetzel, R.; Lednev, I. K. Structural Variations in the Cross-β Core of Amyloid β Fibrils Revealed by Deep UV Resonance Raman Spectroscopy. *J. Am. Chem. Soc.* **2010,** *132*, 6324–6328.

(85) Sikirzhytski, V.; Topilina, N. I.; Higashiya, S.; Welch, J. T.; Lednev, I. K. Genetic Engineering Combined with Deep UV Resonance Raman Spectroscopy for Structural Characterization of Amyloid-Like Fibrils. *J. Am. Chem. Soc.* **2008,** *130*, 5852–5853.

(86) Shashilov, V. A.; Sikirzhytski, V.; Popova, L. A.; Lednev, I. K. Quantitative Methods for Structural Characterization of Proteins Based on Deep UV Resonance Raman Spectroscopy. *Methods* **2010,** *52*, 23–37.

(87) Asher, S. A. Ultraviolet Raman Spectroscopy. In *Handbook of Vibrational Spectroscopy*; Chalmers, J. P., Griffiths, P. R., Eds.; John Wiley & Sons: London, 2002; Vol. 1, pp 557−571.

(88) Kneipp, J.; Balakrishnan, G.; Chen, R.; Shen, T. J.; Sahu, S. C.; Ho, N. T.; Giovannelli, J. L.; Simplaceanu, V.; Ho, C.; Spiro, T. G. Dynamics of Allostery in Hemoglobin: Roles of the Penultimate Tyrosine H-Bonds. *J. Mol. Biol.* **2006,** *256*, 335–353.

(89) Wu, Q.; Balakrishnan, G.; Pevsner, A.; Spiro, T. G. Histidine Photodegradation During UV Resonance Raman Spectroscopy. *J. Phys. Chem. A* **2003,** *107*, 8047–8051.

(90) Dudik, J. M.; Johnson, C. R.; Asher, S. A. UV Resonance Raman Studies of Acetone, Acetamide, and *N*-Methylacetamide: Models for the Peptide Bond. *J. Phys. Chem.* **1985,** *89*, 3805–3814.

DOI: 10.1021/jz101619f | *J. Phys. Chem. Lett.* **2011,** *2*, 334–344